Bioorganic & Medicinal Chemistry 23 (2015) 4139–4149

Contents lists available at ScienceDirect

Bioorganic & Medicinal Chemistry

journal homepage: www.elsevier.com/locate/bmc

Discovery of potent and selective nonplanar tankyrase inhibiting nicotinamide mimics

Yves Nkizinkiko [a], B. V. S. Suneel Kumar [b], Variam Ullas Jeankumar [b], Teemu Haikarainen [a], Jarkko Koivunen [a], Chanduri Madhuri [b], Perumal Yogeeswari [b], Harikanth Venkannagari [a], Ezeogo Obaji [a], Taina Pihlajaniemi [a], Dharmarajan Sriram [b,*], Lari Lehtiö [a,*]

[a] Faculty of Biochemistry and Molecular Medicine & Biocenter Oulu, University of Oulu, PO Box 5400, FIN-90014 Oulu, Finland
[b] Department of Pharmacy at Birla Institute of Technology and Science-Pilani, Hyderabad campus, Hyderabad 500078, India

ARTICLE INFO

Article history:
Received 26 March 2015
Revised 22 June 2015
Accepted 24 June 2015
Available online 2 July 2015

Keywords:
Tankyrase
Poly(ADP-ribose)polymerase
Inhibition
Cancer
Protein crystallography
Virtual screening
Wnt-signalling

ABSTRACT

Diphtheria toxin-like ADP-ribosyltransferases catalyse a posttranslational modification, ADP-ribosylation and form a protein family of 17 members in humans. Two of the family members, tankyrases 1 and 2, are involved in several cellular processes including mitosis and Wnt/β-catenin signalling pathway. They are often over-expressed in cancer cells and have been linked with the survival of cancer cells making them potential therapeutic targets. In this study, we identified nine tankyrase inhibitors through virtual and in vitro screening. Crystal structures of tankyrase 2 with the compounds showed that they bind to the nicotinamide binding site of the catalytic domain. Based on the co-crystal structures we designed and synthesized a series of tetrahydroquinazolin-4-one and pyridopyrimidin-4-one analogs and were subsequently able to improve the potency of a hit compound almost 100-fold (from 11 μM to 150 nM). The most potent compounds were selective towards tankyrases over a panel of other human ARTD enzymes. They also inhibited Wnt/β-catenin pathway in a cell-based reporter assay demonstrating the potential usefulness of the identified new scaffolds for further development.

1. Introduction

Tankyrases belong to the diphtheria toxin-like ADP-ribosyltransferase (ARTD) protein superfamily also known as poly(ADP-ribosyl)polymerases (PARPs) (EC 2.4.2.30).[1] Human tankyrase 1 (TNKS1/ARTD5/PARP5a) and tankyrase 2 (TNKS2/ARTD6/PARP5b) have a C-terminal catalytic ARTD domain, which is conserved in the protein family and is responsible for modifying target proteins by adding one or more ADP-ribose units to specific residues. TNKS1 and TNKS2 are homologous with 82% sequence identity and have overlapping functions.[2] In addition to the ARTD domain, tankyrases have sterile alpha motifs (SAM) responsible for their oligomerization and five ankyrin repeat clusters (ARC) responsible for recognizing and binding target proteins.[3]

The first indication of the therapeutic potential of tankyrase inhibition arose from the observation that tankyrases control the length of human telomeres by poly-ADP-ribosylating (PARsylating) a shelterin protein complex component TRF1. Shelterin protects telomeres by preventing the access of telomerase to telomeres.[4] PARsylation of TRF1 by tankyrases releases TRF1 from the telomeres and allows telomerase to extend the DNA ends. This system is over-activated in cancer cells leading to an uncontrolled telomere extension.[5] Recently many different functions for tankyrases has been discovered[2,6,7] and these have caused an increasing interest in developing tankyrase inhibitors. Regarding cancer two functions of tankyrases are of special interest. TNKS1 was found in spindle poles during mitosis and it is believed to facilitate the formation of normal spindle structure and function.[8] Disrupting this process might be a way to disturb rapidly dividing cancer cells. Tankyrases also control the Wnt signaling pathway, which is a key survival pathway in many cancer cells. Tankyrases PARsylate Axin, which is an essential protein for the formation of the β-catenin destruction complex: a multiprotein complex controlling β-catenin stability through phosphorylation.[9] The PARsylation of axin destabilizes the destruction complex,

Abbreviations: ADE, adenosine subsite; ARC, ankyrin repeat cluster; ARTD, ADP-ribosyltransferase with diphtheria toxin homology; NI, nicotinamide subsite; PAR, poly(ADP-ribose); PARP, poly(adp-ribose) polymerase; SAM, sterile alpha motif; TNKS, tankyrase; TRF1, telomeric repeat binding factor 1.

* Corresponding authors. Tel.: +91 40 66303506 (D.S.), +358 2 9448 1169 (L.L.).
E-mail addresses: dsriram@hyderabad.bits-pilani.ac.in (D. Sriram), lari.lehtio@oulu.fi (L. Lehtiö).

http://dx.doi.org/10.1016/j.bmc.2015.06.063
0968-0896/

stabilizes β-catenin and leads to the activation of the Wnt signaling pathway.[10] Inhibition of tankyrases, therefore, increases cellular levels of Axin and decreases the levels of β-catenin, which ultimately decreases the oncogenic expression mediated by β-catenin and leads to the inhibition of tumorigenesis.[9,11]

Crystal structures of the catalytic domains of both human tankyrases have been solved,[12,13] which enables rational design of tankyrase inhibitors. Protein crystallography has also helped to rationalize the observed selectivity of some of the inhibitors[14–16] and it has been utilized in the development of several TNKS inhibitor scaffolds.[10,17] The donor NAD^+ binding groove of the ARTD domain has two sub-sites, namely the nicotinamide (NI) and the adenosine (ADE) sites, which have been targeted by inhibitors.[7] The known TNKS inhibitors such as **1**–**4** (Fig. 1a) bind to the NI subsite whereas some inhibitors bind to the ADE subsite.[18,19] Also dual binders interacting with both of the subsites have recently been developed.[20,21] The hit compounds identified in this study bind to the NI subsite similarly to several other previously characterized ARTD inhibitors, such as **1** (XAV939). We utilized the available structural data in structure-based virtual screening approach with an aim to identify new tankyrase inhibitor scaffolds. The initial hit compounds were further developed using the existing structural knowledge as a guide for compound synthesis. Structure–activity relationship and tankyrase selectivity was rationalized with the help of protein crystallography. We demonstrate the selectivity of the new inhibitors and show that the compounds are active in a cell-based reporter assay.

2. Materials and methods

2.1. Virtual screening and docking

Energy-based pharmacophore modelling (E-pharmacophore) is a combined effort of pharmacophore perception and protein-ligand interaction energies. E-pharmacophore is computed by docking simulation and the pharmacophore features are then ranked based on their site scores. Here, the E-pharmacophore model was generated from the co-crystal of **1** complexed with TNKS2 and it was subjected to re-docking studies (PDB code 3KR8). This structure was selected as it is a high resolution complex structure of a highly potent compound (XAV939) with TNKS2, which is also used in the biochemical testing of the compounds. The RMSD between the docked pose and crystal conformation is 0.95 Å with glide score of −9.52. It indicates the docking reliability in terms of reproducing the experimentally observed binding mode. The detailed methodology of E-pharmacophore modelling, docking, and ROCS modelling is discussed in Supporting information.

Glide XP (extra precision) module of Schrödinger 9.2 (Glide, version 5.7, Schrödinger, LLC, New York, NY, 81 2011) was utilized for docking. TNKS2–**1** complex structure (PDB: 3KR8) was used for docking of compounds. The protein was prepared using protein preparation wizard and glide energy grids were generated for the prepared protein complex. The binding site was defined by a rectangular box surrounding the ligand (**1**). The ligand was refined using the 'Refine' option in Glide, and the option 70 to output Glide XP descriptor information was chosen (Glide 71 v5.7, Schrodinger, LLC, New York, NY). For the refinement and docking calculations, the default settings as available in the software package were used. The results from the re-docking studies were used for E-pharmacophore modelling.

The generated E-pharmacophore model was further validated by enrichment factor (EF) studies in screening a database. A small library, consisting of 250 tankyrase inhibitors were divided into three bins based on activity range, either highly active (<1 μM), moderately active (1–10 μM) or inactive (>10 μM). Database screening was done by using the pharmacophore model to validate the predictive power of the model. The results were analyzed using a set of parameters such as hit list (Ht), number of active percent of

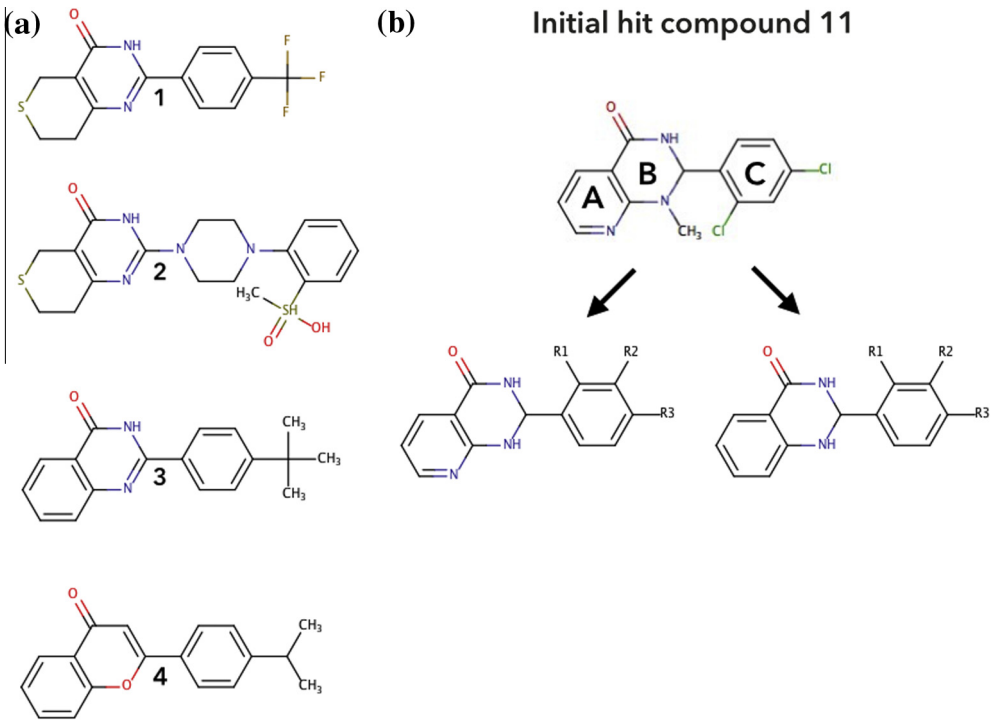

Figure 1. (a) Chemical structure of known tankyrase inhibitors binding to the NI site: **1** XAV939,[13] **2** G244-LM,[38] **3** 2(*tert*-butylphenyl)-3,4-dihydroquinazolin-4-one[15] and **4** 2-4-(propan-2-yl)phenyl-3,4-dihydro-2*H*-1,3-benzoxazin-4-one.[14,30] (b) Schematic representation of **11** and the scaffolds of synthesized pyridopyrimidinone and dihydroquinazolines analogs. The R1, R2 and R3 represent the *ortho*-, *meta*- and *para*-position, respectively, where substitutions were made.

yields (%Y), percent ratio of actives in the hit list (%A), enrichment factor (EF), false negatives, false positives, and goodness of hit score (GH). E-pharmacophore model succeeded in the retrieval of 177 actives (88.5%) of the 200 hits.

The validated pharmacophore model was used as 3D query to screen a commercial database (Asinex) of 4,000,000 compounds to identify potential hits. Top 5000 hits were selected based on the pharmacophore feature mapping and visual inspection. The selected hits were re-ranked using the ROCS model to investigate how similar the hit compounds are to the top active **1** in terms of shape and features. The ROCS model was generated using the redocked conformation of the compound **1** and evaluated further based on the model ranking (enrichment factor) to the known tankyrase inhibitors and decoys. The re-ranked hit list from ROCS was visually inspected and the top diversified hits were chosen based on the ROCS Rank and Tanimoto combo score before being subjected to docking studies. The hit compounds were shortlisted again based on the docking scores and interaction patterns.

2.2. Synthesis and chemicals

All commercially available chemicals and solvents were used without further purification. TLC experiments were performed on alumina-backed silica gel 40 F254 plates (Merck, Darmstadt, Germany). The homogeneity of the compounds was monitored by thin layer chromatography (TLC) on silica gel 40 F254 coated on aluminum plates, visualized by UV light and $KMnO_4$ treatment. Biotage Microwave reactor Initiator was utilized for developing compounds **14**, **16**, **18**, **20**, **22**, **24**, **26**, **28**, **30**, **32**, **34** and **36**. All ^1H and ^{13}C NMR spectra were recorded on a Bruker AM-300 (300.12 MHz, 75.12 MHz) NMR spectrometer, Bruker BioSpin Corp, Germany. Molecular weights of the synthesized compounds were checked by LCMS 6100B series Agilent Technology. Chemical shifts are reported in ppm (δ) with reference to the internal standard TMS. The signals are designated as follows: s, singlet; d, doublet; dd, doublet of doublets; t, triplet; m, multiplet. Elemental analyses were carried out on an automatic Flash EA 1112 Series, CHN Analyzer (Thermo). The analytical and spectral data (^1H NMR, ^{13}C NMR, mass spectra and elemental analysis) of all the synthesized compounds were in full agreement with the proposed structures.

Compounds **15**, **21**, **29**, **31**, **33**, **35**, **37**,[22] **17**, **19**,[23] **27**,[24] **14**, **28**, **30**, **32**[25] and **34**[26] were all known compounds; spectral data obtained were in agreement with the proposed structures and matched those reported in literature.

2.2.1. General procedure for synthesis of 16, 18, 20, 22, 24, 26, and 36

2-Aminonicotinonitrile (1 equiv), the corresponding aldehyde (1 equiv), 1,8-diazbicyclo [5.4.0] undec-7-ene (DBU) (1 equiv), and 1.5 mL water was added in sequential order in a 5 mL microwave vial, sealed and heated to 100 °C for about 5–10 min. The reaction mixture was then cooled to 28 °C and the precipitate obtained was filtered and re-crystallized from appropriate solvent to give the desired compounds in good yields as mentioned below.

2.2.1.1. 2-(2-Chlorophenyl)-2,3-dihydropyrido[2,3-*d*]pyrimidin-4(1*H*)-one (16). The compound was synthesized according to the above general procedure using 2-aminonicotinonitrile (0.1 g, 0.84 mmol), 2-chlorobenzaldehyde (0.12 g, 0.84 mmol), and DBU (0.1 g, 0.84 mmol) to afford **16** (0.14 g, 63.6%) as off white solid. ^1H NMR ($CDCl_3$) δ_H 5.87 (s, 1H), 6.69–7.91 (m, 6H), 8.14–8.16 (m, 1H). ^{13}C NMR (DMSO-d_6): δ_c 163.7, 158.2, 153.6, 143.9, 137.4, 133.6, 128.9, 128.6, 128.2, 126.9, 115.1, 110.3, 62.9. ESI-MS *m*/*z* 260.2 $(M+H)^+$. Anal Calcd for $C_{13}H_{10}ClN_3O$; C, 60.12; H, 3.88; N, 16.18. Found: C, 60.01; H, 3.81; N, 16.24.

2.2.1.2. 2-(*o*-Tolyl)-2,3-dihydropyrido[2,3-*d*]pyrimidin-4(1*H*)-one (18). The compound was synthesized according to the above general procedure using 2-aminonicotinonitrile (0.1 g, 0.84 mmol), 2-methylbenzaldehyde (0.1 g, 0.84 mmol), and DBU (0.1 g, 0.84 mmol) to afford **18** (0.13 g, 65%) as off white solid. ^1H NMR ($CDCl_3$) δ_H 2.34 (s, 3H), 5.83 (s, 1H), 6.71–7.89 (m, 6H), 8.16–8.17 (m, 1H). ^{13}C NMR (DMSO-d_6): δ_c 163.7, 158.4, 153.1, 145.5, 137.6, 135.2, 130.6, 126.9, 126.3, 125.8, 114.8, 110.1, 63.7, 18.7. ESI-MS *m*/*z* 240.1 $(M+H)^+$. Anal Calcd for $C_{14}H_{13}N_3O$; C, 70.28; H, 5.48; N, 17.56. Found: C, 70.19; H, 5.38; N, 17.51.

2.2.1.3. 2-(2-Fluorophenyl)-2,3-dihydropyrido[2,3-*d*]pyrimidin-4(1*H*)-one (20). The compound was synthesized according to the above general procedure using 2-aminonicotinonitrile (0.1 g, 0.84 mmol), 2-fluorobenzaldehyde (0.136 g, 0.84 mmol), and DBU (0.1 g, 0.84 mmol) to afford **20** (0.12 g, 60%) as off white solid. ^1H NMR ($CDCl_3$) δ_H 5.86 (s, 1H), 6.74–7.88 (m, 6H), 8.13–8.14 (m, 1H). ^{13}C NMR (DMSO-d_6): δ_c 163.5, 158.7, 156.4, 152.9, 137.9, 130.2, 128.7, 128.4, 123.8, 115.1, 112.1, 109.6, 62.3. ESI-MS *m*/*z* 244.1 $(M+H)^+$. Anal Calcd for $C_{13}H_{10}FN_3O$; C, 64.19; H, 4.14; N, 17.28. Found: C, 64.27; H, 4.07; N, 17.21.

2.2.1.4. 2-(2-(Benzyloxy)phenyl)-2,3-dihydropyrido[2,3-*d*]pyrimidin-4(1*H*)-one (22). The compound was synthesized according to the above general procedure using 2-aminonicotinonitrile (0.1 g, 0.84 mmol), 2-benzyloxybenzaldehyde (0.18 g, 0.84 mmol), and DBU (0.1 g, 0.84 mmol) to afford **22** (0.12 g, 42.9%) as off white solid. ^1H NMR ($CDCl_3$) δ_H 5.19 (s, 2H), 5.85 (s, 1H), 6.71–7.92 (m, 11H), 8.16–8.18 (m, 1H). ^{13}C NMR (DMSO-d_6): δ_c 163.3, 157.6, 154.5, 152.7, 137.8, 136.9, 128.9, 128.2, 127.9, 127.6, 127.3, 123.8, 121, 114.3, 111.8, 109.6, 70.2, 63.1. ESI-MS *m*/*z* 332.1 $(M+H)^+$. Anal Calcd for $C_{20}H_{17}N_3O_2$; C, 72.49; H, 5.17; N, 12.68. Found: C, 72.58; H, 5.24; N, 12.74.

2.2.1.5. 2-(3-(Benzyloxy)phenyl)-2,3-dihydropyrido[2,3-*d*]pyrimidin-4(1*H*)-one (24). The compound was synthesized according to the above general procedure using 2-aminonicotinonitrile (0.1 g, 0.84 mmol), 3-benzyloxybenzaldehyde (0.18 g, 0.84 mmol), and DBU (0.1 g, 0.84 mmol) to afford **24** (0.13 g, 46.4%) as off white solid. ^1H NMR ($CDCl_3$) δ_H 5.23 (s, 2H), 5.82 (s, 1H), 6.69–7.87 (m, 11H), 8.19–8.20 (m, 1H). ^{13}C NMR (DMSO-d_6): δ_c 162.7, 157.8, 157.4, 153, 148.9, 137.6, 136.9, 129.4, 128.7, 127.7, 126.9, 114.6, 113.9, 111.8, 110.6, 109.7, 69.1, 64.8. ESI-MS *m*/*z* 332.1 $(M+H)^+$. Anal Calcd for $C_{20}H_{17}N_3O_2$; C, 72.49; H, 5.17; N, 12.68. Found: C, 72.41; H, 5.13; N, 12.61.

2.2.1.6. 2-(4-(Benzyloxy)phenyl)-2,3-dihydropyrido[2,3-*d*]pyrimidin-4(1*H*)-one (26). The compound was synthesized according to the above general procedure using 2-aminonicotinonitrile (0.1 g, 0.84 mmol), 4-benzyloxybenzaldehyde (0.18 g, 0.84 mmol), and DBU (0.1 g, 0.84 mmol) to afford **26** (0.15 g, 53.5%) as off white solid. ^1H NMR ($CDCl_3$) δ_H 5.21 (s, 2H), 5.81 (s, 1H), 6.68–6.74 (m, 3H), 7.32–7.89 (m, 8H), 8.15–8.16 (m, 1H).^{13}C NMR (DMSO-d_6): δ_c 162.9, 157.5, 154.8, 152.8, 137.6, 136.9, 136.7, 129.2, 128, 127.6, 127.3, 113.9, 112.8, 109.4, 69.9, 65.1. ESI-MS *m*/*z* 332.2 $(M+H)^+$. Anal Calcd for $C_{20}H_{17}N_3O_2$; C, 72.49; H, 5.17; N, 12.68. Found: C, 72.57; H, 5.19; N, 12.76.

2.2.1.7. 2-(4-(*tert*-Butyl)phenyl)-2,3-dihydropyrido[2,3-*d*]pyrimidin-4(1*H*)-one (36). The compound was synthesized according to the above general procedure using 2-aminonicotinonitrile (0.1 g, 0.84 mmol), 4-*tert*-butylbenzaldehyde (0.136 g, 0.84 mmol), and DBU (0.128 g, 0.84 mmol) to afford **36** (0.14 g, 58.3%) as off white solid. ^1H NMR ($CDCl_3$) δ_H 1.29 (s, 9H), 5.79 (s, 1H), 6.69–7.83 (m, 6H), 8.13–8.15 (m, 1H). ^{13}C NMR (DMSO-d_6): δ_c 163.1, 157.6, 153.6, 152.9, 141.8, 137.7, 125.1, 124.4, 114.3, 109.8, 65.1,

39.6, 36.4. ESI-MS *m*/*z* 282.1 $(M+H)^+$. Anal Calcd for $C_{17}H_{19}N_3O$; C, 72.57; H, 6.81; N, 14.94. Found: C, 72.49; H, 6.73; N, 14.98.

2.2.2. General procedure for synthesis of 23 and 25

The synthesis followed the literature procedure.[22] Cyanuric chloride (10 mol %) was added to a solution of anthranilamide (1 equiv) and desired aldehyde (1 equiv) in acetonitrile (2 mL). The reaction mixture was then stirred at 28 °C for about 15 min (monitored by TLC & LCMS for completion) and allowed to cool. Solvent was evaporated off and the precipitate formed was filtered and re-crystallized form ethanol to afford the desired product as described below.

2.2.2.1. 2-(2-(Benzyloxy)phenyl)-2,3-dihydroquinazolin-4(1*H*)-one (23). The compound was synthesized according to the above general procedure using anthranilamide (0.1 g, 0.73 mmol), 2-benzyloxy benzaldehyde (0.15 g, 0.73 mmol), and cyanuric chloride (0.013 g, 0.073 mmol) to afford **23** (0.13 g, 54%) as white solid. ^{1}H NMR ($CDCl_3$) δ_H 5.21 (s, 2H), 6.01 (s, 1H), 6.88–7.69 (m, 13H) ^{13}C NMR (DMSO-d_6): δ_c 165.3, 157.1, 144.9, 136.5, 133.2, 129.1, 128.4, 127.8, 127.6, 127.5, 126.9, 123.8, 121, 117.1, 116.7, 113.8, 111.8, 70.9, 64.8. ESI-MS *m*/*z* 331.2 $(M+H)^+$. Anal Calcd for $C_{21}H_{18}N_2O_2$; C, 76.34; H, 5.49; N, 8.48. Found: C, 76.31; H, 5.54; N, 8.42.

2.2.2.2. 2-(3-(Benzyloxy)phenyl)-2,3-dihydroquinazolin-4(1*H*)-one (25). The compound was synthesized according to the above general procedure using anthranilamide (0.1 g, 0.73 mmol), 3-benzyloxy benzaldehyde (0.15 g, 0.73 mmol), and cyanuric chloride (0.013 g, 0.073 mmol) to afford **25** (0.11 g,, 45.8%) as off white solid. ^{1}H NMR ($CDCl_3$) δ_H 5.24 (s, 2H), 5.99 (s, 1H), 6.84–7.63 (m, 13H) ^{13}C NMR (DMSO-d_6): δ_c 165.6, 160.7, 145.8, 145.3, 136.4, 133.2, 129.8, 128.6, 128.1, 127.6, 126.8, 118.6, 116.9, 116.5, 113.8, 112.5, 110.9, 70.6, 66.7. ESI-MS *m*/*z* 331.1 $(M+H)^+$. Anal Calcd for $C_{21}H_{18}N_2O_2$; C, 76.34; H, 5.49; N, 8.48. Found: C, 76.39; H, 5.42; N, 8.54.

2.3. Expression and purification of the enzymes

The human ARTDs used during this study were expressed and purified as described shortly below and as reported earlier.[15,27] ARTD1-3 were expressed as full length proteins.[27] For other proteins, the constructs used consisted of catalytic protein fragments: ARTD4 (residues 250–565), TNKS1/ARTD5 (1030–1317), TNKS2/ARTD6 (952–1161 and 873–1161), ARTD7 (460–656) and ARTD10 (809–1017).[27–29] All proteins were purified using a similar protocol as described before.[28,30] Cells were lysed with sonication in the presence of protease inhibitors and the proteins were purified using Ni-affinity, TEV-cleavage of the tag and size exclusion chromatography. A heparin column was additionally used in case of ARTD1-3 in order to remove protein bound DNA fragments. Cloning of ARTD3 and detailed protocols for production of recombinant ARTD3 and TNKS2 used in the assays are given in the Supporting information.

2.4. Activity assay

Assays based on quantification of NAD^+ were conducted as we have reported earlier.[14,28] Reactions were carried out in 96-well plates (Greiner bio-one U-shaped) at room temperature. The buffer used for TNKS2 consisted of 50 mM BisTris propane, pH 7, 0.5 mM TCEP and 0.01% Triton-X-100 and 500 nM of substrate NAD^+ (in 50 μL reaction volume). After the reaction 20 μL of 20% acetophenone in ethanol and 20 μL of 2 M KOH were added and the plate was incubated for 10 min after which 90 μL of formic acid was added. The plates were recorded after 20 min of incubation using Tecan Infinity M1000 plate reader (excitation/emission, 372 nm/444 nm).

2.5. Screening of inhibitors and measurement of inhibitor potencies

All compounds were stored at −20 °C in DMSO and diluted in the TNKS2 assay buffer before use. The preliminary screening was done at 10 μM and 1 μM concentrations in duplicates. Furthermore, compound controls were used to exclude the effect of compound fluorescence and quenching. Inhibitor potencies were measured for the hit compounds that had IC_{50} values below 100 μM based on the two point preliminary screening. IC_{50} values were measured using half log dilutions and reactions were carried in quadruplicates on three separate days. The incubation time was adjusted so that substrate conversion was 50–60% in the case of screening and less than 30% in the case of IC_{50} measurements. Dose response curves for the compounds were measured using a half-log dilutions and fitted using 4-parameters with Graphpad Prism (version 5.0 for windows).

2.6. Profiling of the inhibitors

Selected TNKS2 inhibitors were profiled against a panel of human ARTDs using optimized assay conditions (Supporting information).[27] In order to keep the conditions comparable the concentration of NAD^+ was kept low (500 nM) during the screening and the profiling assays. A dose response curve was measured once for the best hit compounds using half-log dilutions.

2.7. Crystallization, data collection and refinement

The catalytic domain of TNKS2 (residues 952–1161) was used for crystallization.[14] The crystals were soaked for several days in a solution containing 22% of PEG3350, 0.2 M Lithium sulfate and 0.1 M Tris (pH 8.5) supplemented with 100 μM of the compound and with 250 mM NaCl. After soaking the crystals were dipped in the soaking solution supplemented with 20% glycerol, and flash frozen in liquid nitrogen.[19] The data was collected at ESRF (Grenoble, France) on beamline ID23-1 and at Diamond Light source (UK, Didcot) beamlines I02 and I03. The data were processed with XDS[31] (Supporting information) and the molecular replacement was done with MOLREP[32] using TNKS2 structure complexed with nicotinamide as a template (3U9H). Structures were refined with REFMAC5[33,34] and manual building and analysis was done with Coot.[35] The chemical structures of the compounds were drawn with Marvin (Marvin 5.7.0, 2011, ChemAxon, http://www.chemaxon.com).

2.8. Reporter assay

HEK293, L Wnt-3a and L cells (ATCC) were cultured in Dulbecco's modified Eagle's medium supplemented with 10% fetal bovine serum, penicillin and streptomycin at 37 °C in a 5% CO_2 atmosphere. Preparation of Wnt3a and control conditioned medium (CM) has been described previously.[36] HEK293 cells were plated on 96-well plate (2.5×10^4 cells/well) 16 hours before transfection. Cells were transfected with SuperTopFlash reporter plasmid[37] at the same time with pCMV-ß-galactosidase plasmid (Clontech) using the FuGENE™ 6 Transfection Reagent (Roche) according to the manufacturer's protocol. Following transfection, cells were incubated 24 hours with 50% of Wnt3a-CM or control-CM in serum free DMEM containing molecules or DMSO vehicle. DMSO content was kept below 0.05% in all experiments. Cells were washed once with PBS, lysed and Wnt3a induced luciferase activity was measured using the Luciferase assay system (Promega)

according to manufacturer's instructions. β-Galactosidase activity was measured using the β-galactosidase enzyme assay system (Promega) to normalize the transfection efficiency. The results are the mean of three independent experiments ± SEM. Overall, the compounds did not affect the luciferase activity when control medium was used and the control conditioned medium had no significant effect on the luciferase activity. Cell viability was also controlled with light microscope.

3. Results

3.1. Virtual screening and design

We utilized structure and analogue-based approaches to identify potential tankyrase inhibitors. In the first approach, Energy-based pharmacophore model (E-pharmacophore) was generated by utilizing the existing protein-ligand interaction information. The E-pharmacophore model was validated using TNKS2–**1** complex crystal structure (PDB: 3KR8) and a tankyrase inhibitor library, and the model was then used as query to commercial (Asinex) database (Fig. 2). Top hits from the pharmacophore screening were prioritized by shape and feature similarity with the top active (**1**) using a ROCS model. The selected compounds were subjected to docking studies to predict the binding modes and to reduce the number of false positives. 9 hits were carefully selected based on the E-pharmacophore, ROCS ranking and docking analysis and they were screened for tankyrase inhibition.

Six of the 9 hit compounds had an IC_{50} below 11 μM and three of the six had potencies lower than 1 μM (Table 1). The most potent hit compounds, **5** and **6**, are both derivates of 2-(piperazin-1-yl)-5,6,7,8-tetrahydro-3*H*-quinazolin-4-one. Interestingly pyridopyrimidinones **7**–**13** all had potencies in the μM range, although these compounds do not have an aromatic structure typically reported for ARTDs and tankyrase inhibitors.[7,15]

3.2. Crystal structures of the hit compounds in complex with TNKS2

In order to understand and verify the molecular details of the compound interactions we solved co-crystals structures of the key compounds with TNKS2 catalytic domain. As expected, **5** and **6** bind to the NI subsite (Fig. 3a and b). They form π–π interaction with Tyr1071 and hydrogen bonds to the backbone of Gly1032 and to the side chain hydroxyl of Ser1068. These compounds extend along the NAD^+ binding crevice towards the Phe1035 and the piperazine moiety forms hydrophobic interactions with Ile1075 of the hydrophobic nook and Tyr1050 of the D-loop. Similarly they interact with the Phe1035 at the delta of the cleft. Compound **5** extends towards the D-loop with the pyridine moiety and replaces a water molecule, but does not make direct interactions with the protein. There is a 15° rotation of Phe1035 with respect to the compound **6** complex structure and the D-loop moves 1 Å in order to accommodate the bulkier compound **5** (Fig. 3a and b). Both **5** and **6** showed a similar binding mode in the docking studies.

In contrast to **5** and **6**, compounds **8**, **9**, **10** and **11** contain a nonaromatic B-ring and therefore represent an unconventional PARP inhibitor scaffold (Table 1, Fig. 1b). We wanted to, despite the modest potency, to characterize this series further. We solved

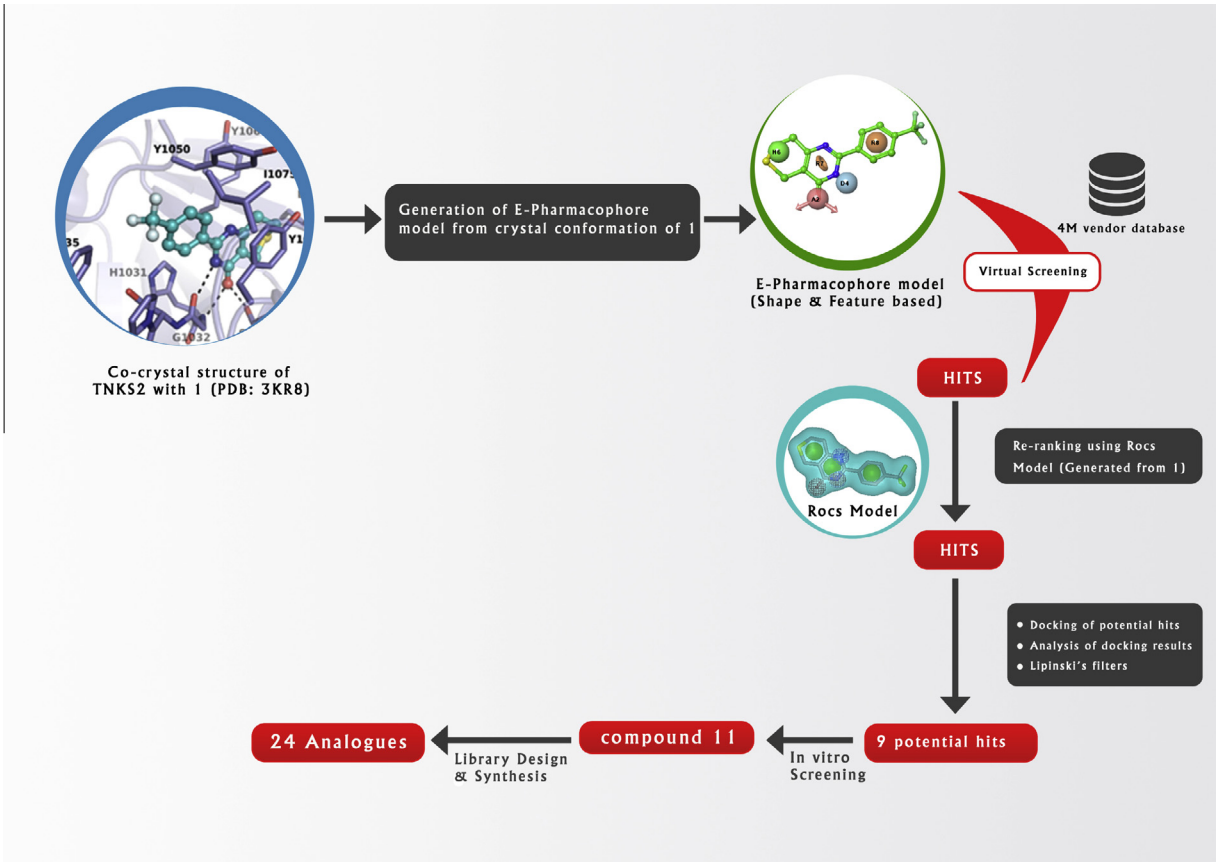

Figure 2. Virtual and in vitro screening workflow. The virtual screening was based on the co-crystal structure (3KR8) of compound **1** (XAV939) with TNKS2. The binding mode of **1** was used to create an E-pharmacophore model, which was used to screen 4 million compounds from vendor databases. Using the ROCS model generated for **1**, the initial hits were re-ranked and 9 final hit compounds were identified for further in vitro studies. Crystallography was used to study co-crystal structures of TNKS2 with the most potent hit compounds and this lead to the synthesis of a series of analogues which have improved potency against TNKSs.

Table 1
Potencies of the hit compounds against TNKS2

Compound (PDB code)	Structure	TNKS2 IC_{50} (pIC_{50} ± SEM)
5 (5AL5)	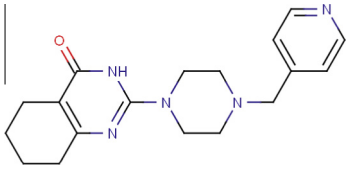	71 nM (7.15 ± 0.04), *n* = 3
6 (5AL4)	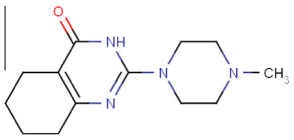	300 nM (6.52 ± 0.05), *n* = 3
7	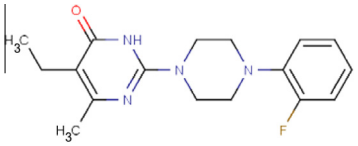	720 nM (6.14 ± 0.05), *n* = 3
8	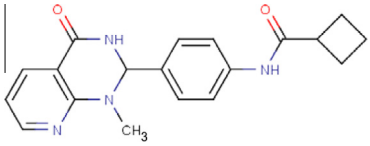	2300 nM (5.63 ± 0.05), *n* = 3
9	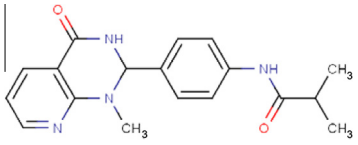	6200 nM (5.2 ± 0.08), *n* = 3
10	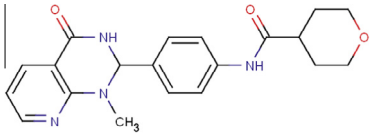	6600 nM (5.0 ± 0.06), *n* = 3
11 (5AL3)	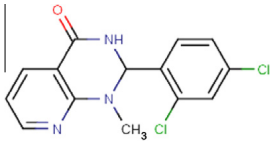	11,000 nM (5.0 ± 0.03), *n* = 3
12	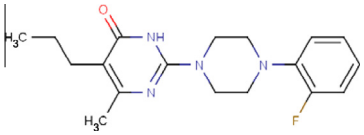	64,000 nM (4.2 ± 0.38), *n* = 3
13	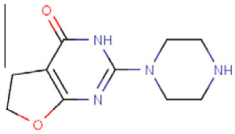	>100,000 nM

a crystal structure of TNKS2 with **11** containing the chlorine substituents at the benzene ring. The potency of this nonplanar scaffold is reduced likely due to the missing capacity to form a π–π interaction with Tyr1071. Compound **11** binds also to the NI subsite and forms the typical hydrogen bonds (Fig. 3c). The compound is a racemic mixture, but we clearly identified only the R-enantiomer in the crystal structure. The N-methyl group of the B-ring interacts with the Tyr1050. Interestingly, the N-methyl group and the *ortho*-chlorine substituent of the benzene ring (C-ring) caused a 90° degree rotation of the C-ring unique for this scaffold (Fig. 3c and d). Chlorine replaces water molecule hydrogen bonded to the backbone amide of Tyr1050. Chlorine at the *para*-position interacts with the Phe1035. We have previously shown that this hydrophobic interaction is a potential way to increase affinity and selectivity of the inhibitors.[14,15] The crystal structures revealed that the rotation of the C-ring of **11** and the presence of *para*-chlorine caused Tyr1050 and Phe1035 to move away from the compound but the overall structure of the binding pocket did not change (Fig. 3b and c).

3.3. Derivatives

3.4.1. Synthesis

The identified compounds are analogous to **1**,[9] to **2**,[38] **3**[15,39] and to **4**[14,30] (Fig. 1a). We were intrigued by the inhibition of tankyrases by pyridopyrimidinones containing a chiral center and lacking the aromatic B-ring. Therefore, using our earlier efforts to create tankyrase selective flavones[30] and dihydroquinazolinones[15] as guides, we decided to synthesize analogs of pyridopyrimidinones. N-methyl group of **11** is restricting the conformation of the phenyl group and it was removed from the compound at this stage (Fig. 1b). Derivatives were designed by making systematic substitution either at *ortho*- or *meta*- or *para*-positions at the C-ring (Fig. 1b).

The synthesis of 2-(sub)aryl-2,3-dihydroquinazolin-4(1*H*)-one and 2-(sub)aryl-2,3-dihydropyrido[2,3-*d*]pyrimidin-4(1*H*)-one derivatives has been well precedent in literature. A series of 12 quinazolinone and 12 pyridopyrimidinone analogues were synthesized by a straightforward methodology as depicted in Scheme 1, as step towards derivation of a strong structure-activity relationship and to understand the ideal site for introducing structural diversity. 2-(sub)aryl-2,3-dihydroquinazolin-4(1*H*)-one analogues compounds **15**, **21**, **23**, **25**, **29**, **31**, **33**, **35** and **37** were synthesized using cyanuric chloride catalyzed protocol as previously reported by Sharma et al.[22] Propylphosphoric anhydride mediated method was employed for developing compounds **17** and **19**.[23] Compound **27** was synthesized by condensing anthranilamide and 4-benzyloxy benzaldehyde in ethanol utilizing catalytic amount of ammonium chlolride.[24] 2-(sub)aryl-2,3-dihydropyrido[2,3-*d*]pyrimidin-4(1*H*)-one derivatives (compounds **14**, **16**, **18**, **20**, **22**, **24**, **26**, **28**, **30**, **32**, **34** and **36**) were generated utilizing a 1,8-diazbicyclo [5.4.0] undec-7-ene (DBU) catalyzed microwave assisted synthesis as previously described by Yang et al.[25]

3.4.2. Evaluation of the analogs

Seven different substituents were used to modify the two starting scaffolds, pyridopyrimidinone **14** and tetrahydroquinazolinone **15**. In total, 24 analogs were generated (Table 2). The main difference between the two series of analogs is the presence of nitrogen in the pyrimidine-ring (A-ring), whose removal increased the lipophilicity of the compounds (Table 2). In general, the tetrahydroquinazolinones show slightly better potency against TNKS2 (Table 2). Compared to the initial starting compound **11** the most potent compound of the two series, **37**, was a significant improvement in potency from 11 μM to 150 nM (Table 2).

3.4.3. Structure activity relationships

The crystal structures of TNKS2 complexes with selected four compounds are reported here to illustrate the interaction between the TNKS2 and the analogs (Fig. 4). The tetrahydroquinazolinone analogs made same hydrogen bonds as those observed with **5** and **6** whereas the pyridopyrimidinone analogs, in addition to the typical hydrogen bonds, formed an additional hydrogen bond between the A-ring nitrogen and a water molecule found in the vicinity only in these crystal structures (Fig. 4b and c). Similar hydrogen bond was also formed by **11** (Fig. 3c). The *para*-substituted analogs were more potent than the *ortho*- and *meta*-substituted ones and this observation can be explained by the observation that the *para*-substitution caused the compound to extend outwards along the NAD^+ binding cavity and form

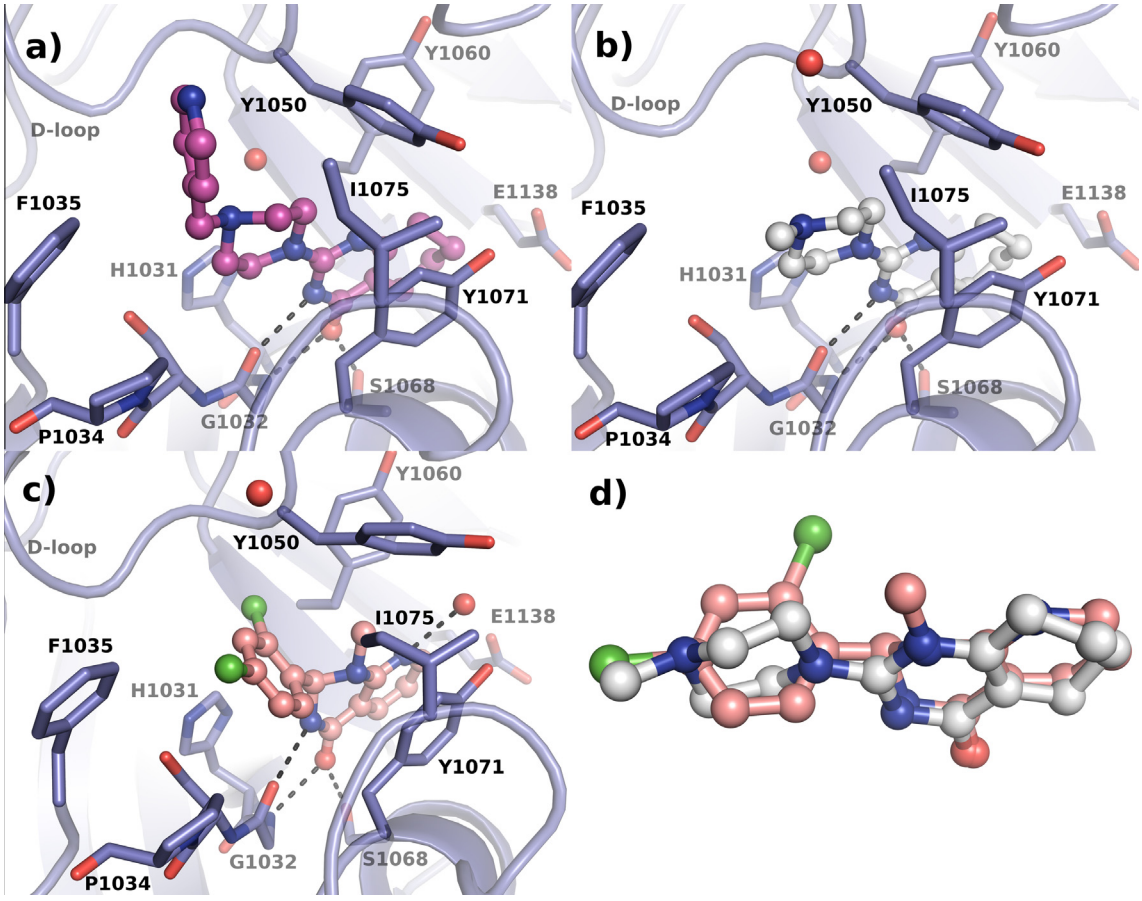

Figure 3. The binding modes of initial hit compounds to TNKS2. Panels show the observed binding modes of (a) **5**, (b) **6**, and (c) **11**. (d) Shows the superposition of compounds **6** and **11** as observed in the crystal structures. Inhibitors are shown in ball and stick models, water molecules as red spheres, surrounding residues as sticks, and hydrogen bonds as dashed lines.

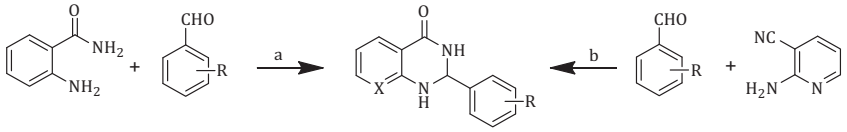

X = N, for compounds 14, 16, 18, 20, 22, 24, 26, 28, 20, 32, 34 and 36
X = C, for compounds 15, 17, 19, 21, 23, 25, 27, 29, 31, 33, 35 and 37

a. Cyanuric chloride 10mol%, CH_3CN, 27°C (for compounds 15,21,23,25,29,31,33,35 and 37); Propylphosphonic anhydride (50% in EtOAc), CH_3CN, 27°C (for compounds 17,19); NH_4Cl (cat:), C_2H_5OH, 27°C (for compound 27); b. 1,8 - diazbicyclo [5.4.0] undec-7-ene H_2O, MW, 100°C (for compounds 14, 16, 18, 20, 22, 24, 26, 28, 30, 32 and 36).

Scheme 1. Synthetic strategy employed for generating compounds **14**–**37**.

enhanced interactions with the protein similarly to **5**. The removal of the *N*-methyl and the *ortho*- and the *para*-chlorine found in **11** was not favorable and resulted in the basic scaffold **14**, which had lower potency of 12 μM. However, the removal of the A-ring nitrogen from **14** yielded **15** that is two fold more potent than **14**. The *ortho*-chlorine substitution at the C-ring in **16** and **17** caused lower potencies and other small substituents in this position **18**–**21** did not improve the potency of the starting compounds **14** and **15**. Interestingly, the potency was improved by the use of a larger *ortho*-substituent, benzyloxy, in **22** and **23**. Benzyloxy substituent decreased the potency when attached to the *meta*-position **24** and **25**, but it is tolerated at the *para*-position (Table 2).

The initial hit compound **11** contained two chlorine substituents and the increased potency of **28** (IC_{50} 760 nM) and **29** (IC_{50} 410 nM) where *para*-chlorine was preserved highlights the importance of the hydrophobic substituent at this position. The hydrophobic interactions made by chlorine in the *para*-position with Phe1035 observed in the crystal structure (Fig. 4a) were clearly favorable compared to the chlorine substitutions at *ortho*-position in **16** and **17**, which have decreased potencies of 31 μM and 140 μM, respectively. Small methyl (**30** and **31**) or methoxy (**32** and **33**) substituents were not beneficial over chlorine (Table 2). Replacement of the *para*-chlorine with a larger aliphatic substituent, isopropyl, increased the hydrophobic interaction of **34** and **35** with Phe1035 (Fig. 3b). This substitution improved the potency 2-fold when comparing the compounds in the same series **28** and **34** as well as **29** and **35**. Consistently the removal of the A-ring nitrogen in tetrahydroquinazolinones improved the potency against TNKS2 (Table 2). Increasing the size of the aliphatic substituent to tert-butyl yielded the most potent analog in the series

Table 2
Potencies of the synthesized analogs against TNKS2. Dose response curves were measured three times for the most active compounds

Compound (PDB code)	Structure	TNKS2 IC_{50} (pIC_{50} ± SEM)	Compound	Structure	TNKS2 IC_{50} (pIC_{50} ± SEM)
14	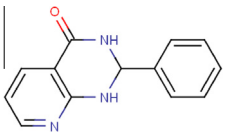	12,000 nM (4.94 ± 0.03)	**15**	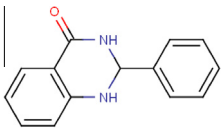	5500 nM (5.26 ± 0.06)
16	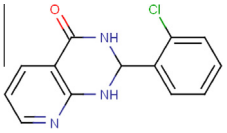	140,000 nM	**17**	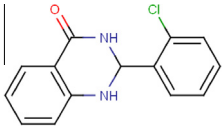	31,200 nM
18	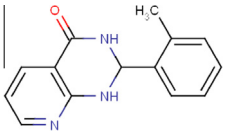	93,000 nM	**19**	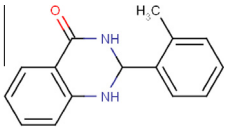	92,000 nM
20	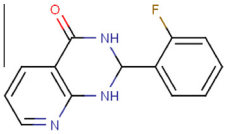	63,000 nM	**21**	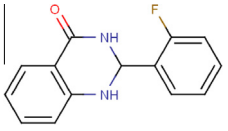	15,000 nM (4.82 ± 0.03)
22	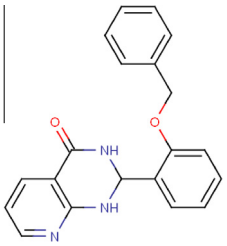	4500 nM (5.35 ± 0.04)	**23**	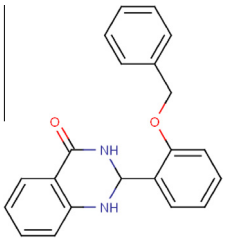	580 nM (6.24 ± 0.05)
24	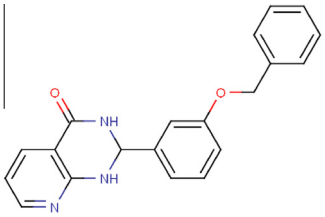	230,000 nM	**25**	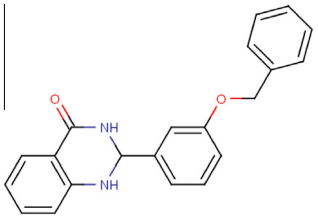	7300 nM (5.14 ± 0.06)
26	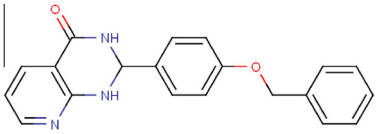	1900 nM (5.71 ± 0.09)	**27**	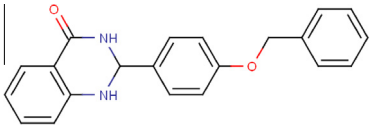	2700 nM (5.57 ± 0.15)
28	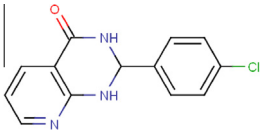	760 nM (6.12 ± 0.10)	**29** (5AKW)	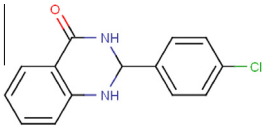	410 nM (6.38 ± 0.28)
30	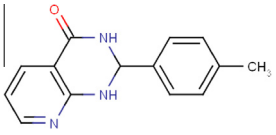	5400 nM (5.27 ± 0.02)	**31**	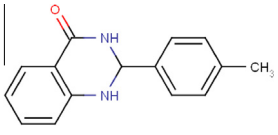	2700 nM (5.57 ± 0.229)
32	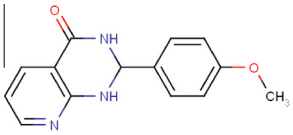	2100 nM (5.67 ± 0.08)	**33**	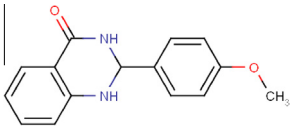	990 nM (6.00 ± 0.147)

Table 2 (*continued*)

Compound (PDB code)	Structure	TNKS2 IC_{50} (pIC_{50} ± SEM)	Compound	Structure	TNKS2 IC_{50} (pIC_{50} ± SEM)
34 (5AL2)	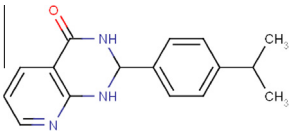	360 nM (6.45 ± 0.07)	**35**	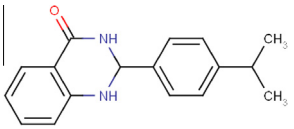	230 nM (6.63 ± 0.06)
36 (5AL1)	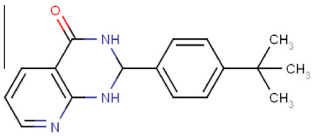	53,000 nM (4.27 ± 0.14)	**37** (5AKU)	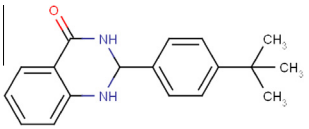	150 nM (6.81 ± 0.18)

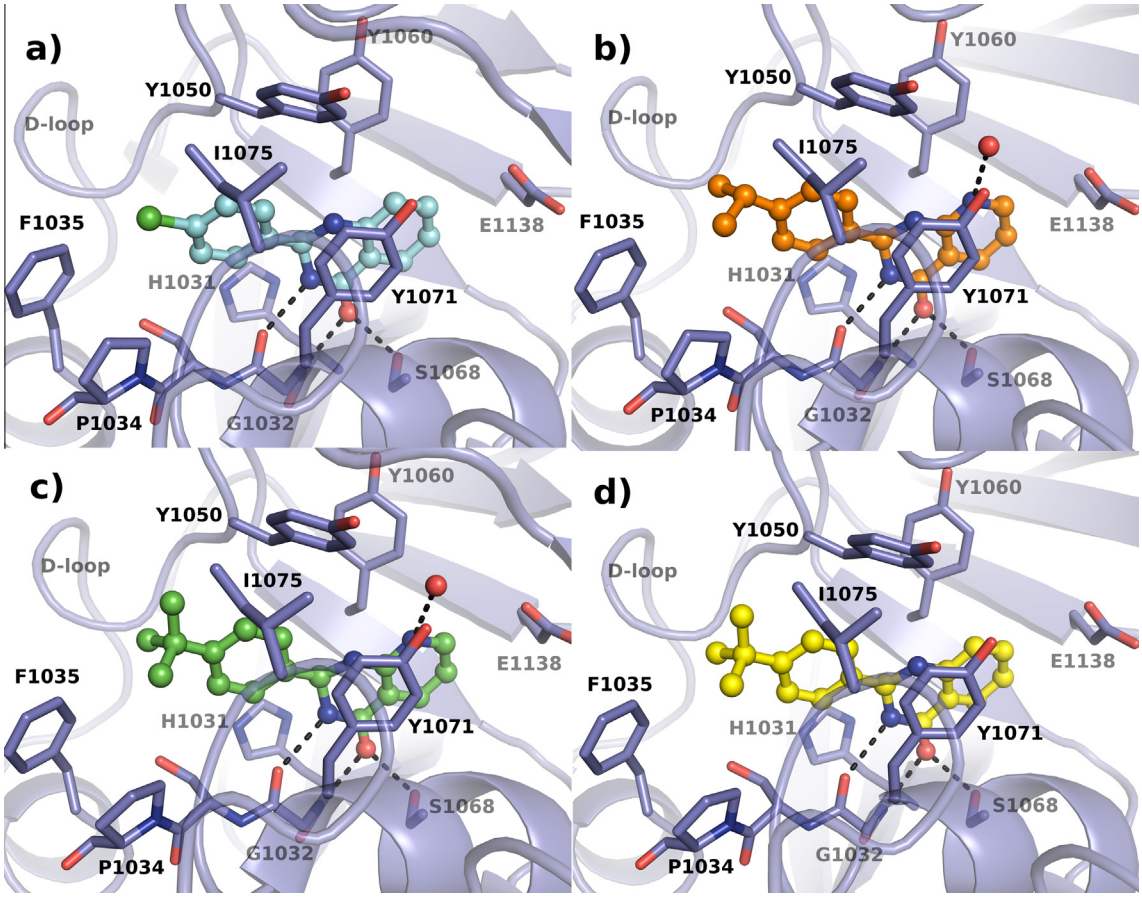

Figure 4. Crystal structures of TNKS2 in complex with the synthesized inhibitors (a) **29**, (b) **34**, (c) **36** and (d) **37**. Inhibitors are shown in ball and stick models, water molecules as red spheres, surrounding residues as sticks, and hydrogen bonds as dashed lines.

(**37**) with IC_{50} of 150 nM, but interestingly **36** showed a remarkably low potency despite the presence of tert-butyl substituent (Table 2). Both **36** and **37** bind to the TNKS2 catalytic domain in a similar manner as demonstrated by the crystal structure (Fig. 4c and d). The only clear difference in the structures is the additional hydrogen bond to a water molecule made by **36**.

Taken together, we noticed that the increase in size and hydrophobicity of the *para*-substituent from *para*-methyl, to *para*-isopropyl and to *para*-*tert*-butyl enhanced the potency of the compound. Furthermore, the removal of the A-ring nitrogen produced compounds, which had even better potency. This led to the removal of the water molecule, increased hydrophobicity and enhanced potency (Figs. 3 and 4). Notably, the most potent compounds have high potency even though they lack the aromatic B-ring found in other potent TNKS inhibitors such as in **1**–**4** (Fig. 1a).

3.4.4. Inhibition of Wnt signaling

The best compounds (**5**, **6**, **35** and **37**) were tested in a SuperTopFlash (STF) based Wnt responsive reporter assay. When the canonical Wnt signaling is activated, β-catenin is stabilized and translocated to the nucleus. In the nucleus, beta-catenin associates with TCF/LEF transcription factors and activates the transcription of Wnt target genes. The STF reporter is Wnt responsive luciferase construct with TCF/LEF binding sites. Thus, the STF assay measures the accumulation of β-catenin, which is controlled by

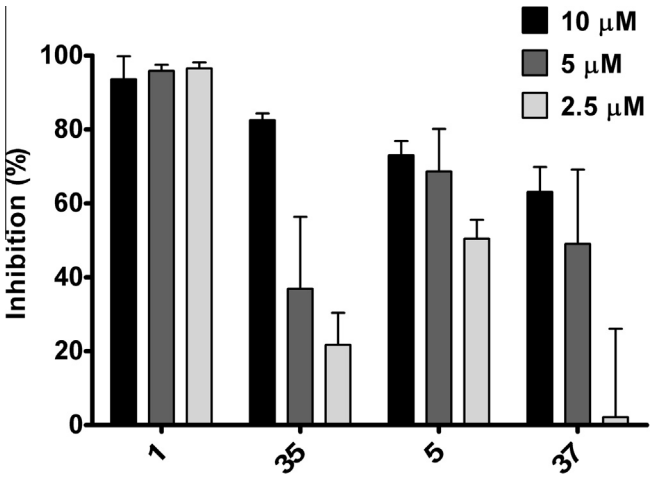

Figure 5. Inhibition of Wnt/β-catenin signaling pathway in STF cell-based reporter assay. Compound **1** also known as XAV939 was used as a control. Dose response with three concentrations is shown for **1**, **5**, **35** and **37**. Compound **6** did not have any response at the tested concentrations and was omitted from the figure. Measurements were done in triplicates and the figure shows the mean value of three independent experiments with SEM.

tankyrases though the stability of the β-catenin destruction complex. STF reporter assay is a widely used method to measure the interference with the Wnt/β-catenin signaling pathway and for the effectiveness of tankyrase inhibitors.[11,14–17] **5**, **35** and **37** were found to be effective Wnt/β-catenin signaling inhibitors at concentration of 10 μM (63–82% inhibition) (Fig. 5). The inhibition is in all cases dose dependent, but does not reach full inhibition of the reporter assay as in the case of highly potent control compound **1**. Interestingly **6** was not effective in this assay at all (data not shown) even though it is a potent TNKS2 inhibitor in vitro. The molecules did not have an effect on β-galactosidase activity and consequently, the compounds do not alter HEK293 cell viability at tested concentrations.

3.4.5. Profiling of the best inhibitors

In order to evaluate the specificity of the best compounds we profiled them against a panel of other ARTD family members. All the tested compounds showed different degrees of selectivity (Table 3). Compound **5** and **6** inhibited also other ARTDs with micromolar IC_{50} values. The potencies of the compounds against TNKS1 and TNKS2 were almost equal except **6**, which has 21-fold selectivity towards TNKS2. This indicates that inhibition of TNKS2 alone would not be enough to inhibit Wnt signaling in the reporter assay (Fig. 5). As **6** is a selective inhibitor of TNKS2 it could be a useful tool to probe differences between tankyrase isoforms. Compounds **35** and **37** were selective towards tankyrases and in most cases we did not observe any inhibition of other tested ARTDs. The potency of **35** and **37** is slightly lower for TNKS1 explaining why the potency in the cell based assay is at the micromolar range. Overall **37** emerged as the most potent and selective compound against tankyrases.

Table 3
Summary of selectivity profiling of the best compounds with IC_{50} against different human ARTDs

	5	6	35	37
TNKS1	370 nM	6.3 μM	1.1 μM	620 nM
TNKS2	71 nM	300 nM	230 nM	150 nM
ARTD1/PARP1	5.9 μM	3.6 μM	>100 μM	>100 μM
ARTD2/PARP2	4.2 μM	3.6 μM	>100 μM	>100 μM
ARTD3/PARP3	13 μM	91 μM	50 μM	34 μM
ARTD4/PARP4	33 μM	17 μM	>100 μM	>100 μM
ARTD7/PARP15	>10 μM	>10 μM	>10 μM*	>10 μM*
ARTD10/PARP10	5.4 μM	>10 μM	>10 μM*	>10 μM*

* No inhibition at the highest concentration used (10 μM).

4. Discussion and conclusion

We conducted the virtual screening in search of new TNKS inhibitor scaffolds based on the known TNKS inhibitors. The virtual screening was successful in that three out of nine initial hits had potencies, which were less than 1 μM. While the most potent compound **5** is analogous to the compound **4** reported earlier, some of the initial hit compounds had a unique scaffold lacking an aromatic B-ring. We wanted to explore this feature by testing pyridopyrimidinones and tetrahydroquinazolinones for tankyrase inhibition. The results showed that the aromaticity of the B-ring is not an absolute requirement for achieving high potency. The synthesized 24 analogs were distinguishable by their substituents in the C-ring and by the presence of the A-ring nitrogen, whose removal increased the hydrophobicity and potency of the compounds. This observation, which is a trend among the 24 analogs, was in compliance with our previously published results regarding the hydrophobicity of potent tankyrase inhibitors.[2,7,19] Furthermore, the obtained structure–activity relationship was in agreement with our previous studies done with other tankyrase inhibitors such as flavones and *para*-substituted 2-phenyl-3,4-dihydroquinazolin-4-ones, which bind to nicotinamide subsite.[15,30] The removal of the A-ring nitrogen and the *ortho*-chlorine from **11** produced nearly *para*llel conformation of the aromatic rings upon binding to TNKS2. The *para*-substitution of the benzene ring was favorable over the *ortho*- and the *meta*-substitution because of the conformational restraint caused by the narrow binding site (Figs. 3 and 4). The substitution at either *ortho*- or *meta*-position would clash with the side chains of Tyr1060, Tyr1050 or His1031, depending on the size of the substituent. However, the *para*-substitution extends the molecule in an opening towards hydrophobic residues Pro1034 and Phe1035 (Fig. 4). In addition, increasing the size of the *para*-substituent from methyl to *tert*-butyl increases the potency of the compounds due to tighter interaction with the Phe1035 and Pro1034 lining the pocket.

The STF cell-based reporter assay revealed that three out of four tested compounds were active in cells with compound **35** having the highest activity. Four compounds were profiled against other human ARTDs and compound **35** and **37** had higher selectivity towards tankyrase than other compounds (Table 3). The hydrophobic *para*-substituent is a source for selectivity as it interacts with a poorly conserved region where, in other ARTDs, they are replaced with hydrophilic residues explaining the observed specificity for tankyrases.[7] In case of, for example, ARTD1 the *para*-substituent would clash with a negatively charged environment of regulatory domain, not present in tankyrases.[15]

Using existing structural information we have been able to identify a new inhibitor scaffold and through synthesis of analogs we were able to improve the potency of the compounds. We also demonstrated the selectivity of the inhibitors towards tankyrases and showed that they are active in cells. The selectivity results from enhanced interactions with the hydrophobic residues Phe1035 and Pro1034 found in tankyrases (Figs. 3 and 4). In other ARTDs this region is more hydrophilic and in case of ARTD1-3 a regulatory domain interacting with the catalytic domain provides further polar environment and causes a selectivity of the hydrophobic *para*-substituted analogs towards tankyrases. We have reported this observation also for other scaffolds.[14,15,40] **37** was identified as the most potent inhibitor in the series with IC_{50}

value of 150 nM for TNKS2 and **6** was demonstrated to have a high selectivity for TNKS2 over TNKS1. Catalytic domains of tankyrases are highly similar and the residues lining the active site are identical. Despite the similarity it is usual for tankyrase inhibitors to display some degree of selectivity for one or the other isoform.[41,42] It is not clear where the selectivity comes from as the crystal structures do not elucidate features that could be responsible for the selectivity. The D-loop adopts different conformations in the crystal structures and also the overall dynamics of the catalytic domains may provide reasons of the selectivity. The crystal structures consist of only the catalytic domain and the SAM domain responsible for the oligomerization could contribute on the selectivity. However, **6** is the most isoform selective compound reported so far and might allow the use of **6** as a chemical probe to decipher the roles of the tankyrase isoforms in various cellular contexts.

PDB codes

Coordinates and structure factors are deposited to the protein data bank with codes 5AL1, 5AL2, 5AL3, 5AL4, 5AL5, 5AKU and 5AKW.

Acknowledgements

The work was funded by Biocenter Oulu, Sigrid Jusélius Foundation, Academy of Finland (Grant No. 266922 for Teemu Haikarainen and 284605 for the Centre of Excellence). This work was carried out with the support of the Diamond Light Source (Didcot, UK) and the European Synchrotron Radiation Facility (ESRF, Grenoble, France). We are grateful to Local Contacts at ESRF and at Diamond for providing assistance in using beamlines ID23-1 and I02, I03, I04-1. The research leading to these results has received funding from the European Community's Seventh Framework Programme (FP7/2007-2013) under BioStruct-X (Grant agreement N° 283570). The use of the facilities and expertise of the Biocenter Oulu core facility, a member of Biocenter Finland and Instruct-FI, is gratefully acknowledged.

Supplementary data

Supplementary Table 1 contains the information regarding data collection and refinement statistics for the crystal structures. Supplementary Table 2 describes the conditions used for each ARTD isoenzyme. Supplementary Table 3 lists the catalogue numbers for the purchased compounds. Supplementary methods describe expression and purification of ARTD3 and TNKS2 and details of the virtual screening protocol. Supplementary data associated with this article can be found, in the online version, at http://dx.doi.org/10.1016/j.bmc.2015.06.063.

References and notes

1. Hottiger, M. O.; Hassa, P. O.; Lüscher, B.; Schüler, H.; Koch-Nolte, F. *Trends Biochem. Sci.* **2010**, *35*, 208.
2. Lehtiö, L.; Chi, N.-W.; Krauss, S. *FEBS J.* **2013**, *280*, 3576.
3. Guettler, S.; LaRose, J.; Petsalaki, E.; Gish, G.; Scotter, A.; Pawson, T.; Rottapel, R.; Sicheri, F. *Cell* **2011**, *147*, 1340.
4. Smith, S.; Giriat, I.; Schmitt, A.; de Lange, T. *Science* **1998**, *282*, 1484.
5. Smith, S.; de Lange, T. *Curr. Biol.* **2000**, *10*, 1299.
6. Riffell, J. L.; Lord, C. J.; Ashworth, A. *Nat. Rev. Drug Discov.* **2012**, *11*, 923.
7. Haikarainen, T.; Krauss, S.; Lehtio, L. *Curr. Pharm. Des.* **2014**.
8. Chang, P.; Coughlin, M.; Mitchison, T. J. *Nat. Cell Biol.* **2005**, *7*, 1133.
9. Huang, S.-M. A.; Mishina, Y. M.; Liu, S.; Cheung, A.; Stegmeier, F.; Michaud, G. A.; Charlat, O.; Wiellette, E.; Zhang, Y.; Wiessner, S.; Hild, M.; Shi, X.; Wilson, C. J.; Mickanin, C.; Myer, V.; Fazal, A.; Tomlinson, R.; Serluca, F.; Shao, W.; Cheng, H.; Shultz, M.; Rau, C.; Schirle, M.; Schlegl, J.; Ghidelli, S.; Fawell, S.; Lu, C.; Curtis, D.; Kirschner, M. W.; Lengauer, C.; Finan, P. M.; Tallarico, J. A.; Bouwmeester, T.; Porter, J. A.; Bauer, A.; Cong, F. *Nature* **2009**, *461*, 614.
10. Bregman, H.; Chakka, N.; Guzman-Perez, A.; Gunaydin, H.; Gu, Y.; Huang, X.; Berry, V.; Liu, J.; Teffera, Y.; Huang, L.; Egge, B.; Mullady, E. L.; Schneider, S.; Andrews, P. S.; Mishra, A.; Newcomb, J.; Serafino, R.; Strathdee, C. A.; Turci, S. M.; Wilson, C.; DiMauro, E. F. *J. Med. Chem.* **2013**, *56*, 4320.
11. Waaler, J.; Machon, O.; Tumova, L.; Dinh, H.; Korinek, V.; Wilson, S. R.; Paulsen, J. E.; Pedersen, N. M.; Eide, T. J.; Machonova, O.; Gradl, D.; Voronkov, A.; von Kries, J. P.; Krauss, S. *Cancer Res.* **2012**, *72*, 2822.
12. Lehtiö, L.; Collins, R.; van den Berg, S.; Johansson, A.; Dahlgren, L.-G.; Hammarström, M.; Helleday, T.; Holmberg-Schiavone, L.; Karlberg, T.; Weigelt, J. *J. Mol. Biol.* **2008**, *379*, 136.
13. Karlberg, T.; Hammarström, M.; Schütz, P.; Svensson, L.; Schüler, H. *Biochemistry* **2010**, *49*, 1056.
14. Narwal, M.; Koivunen, J.; Haikarainen, T.; Obaji, E.; Legala, O. E.; Venkannagari, H.; Joensuu, P.; Pihlajaniemi, T.; Lehtiö, L. *J. Med. Chem.* **2013**, *56*, 7880.
15. Haikarainen, T.; Koivunen, J.; Narwal, M.; Venkannagari, H.; Obaji, E.; Joensuu, P.; Pihlajaniemi, T.; Lehtiö, L. *ChemMedChem* **2013**, *8*, 1978.
16. Voronkov, A.; Holsworth, D. D.; Waaler, J.; Wilson, S. R.; Ekblad, B.; Perdreau-Dahl, H.; Dinh, H.; Drewes, G.; Hopf, C.; Morth, J. P.; Krauss, S. *J. Med. Chem.* **2013**, *56*, 3012.
17. Shultz, M. D.; Majumdar, D.; Chin, D. N.; Fortin, P. D.; Feng, Y.; Gould, T.; Kirby, C. A.; Stams, T.; Waters, N. J.; Shao, W. *J. Med. Chem.* **2013**, *56*, 7049.
18. Karlberg, T.; Markova, N.; Johansson, I.; Hammarström, M.; Schütz, P.; Weigelt, J.; Schüler, H. *J. Med. Chem.* **2010**, *53*, 5352.
19. Narwal, M.; Venkannagari, H.; Lehtiö, L. *J. Med. Chem.* **2012**, *55*, 1360.
20. Bregman, H.; Gunaydin, H.; Gu, Y.; Schneider, S.; Wilson, C.; DiMauro, E. F.; Huang, X. *J. Med. Chem.* **2013**, *56*, 1341.
21. Shultz, M. D.; Cheung, A. K.; Kirby, C. A.; Firestone, B.; Fan, J.; Chen, C. H.-T.; Chen, Z.; Chin, D. N.; Dipietro, L.; Fazal, A.; Feng, Y.; Fortin, P. D.; Gould, T.; Lagu, B.; Lei, H.; Lenoir, F.; Majumdar, D.; Ochala, E.; Palermo, M. G.; Pham, L.; Pu, M.; Smith, T.; Stams, T.; Tomlinson, R. C.; Touré, B. B.; Visser, M.; Wang, R. M.; Waters, N. J.; Shao, W. *J. Med. Chem.* **2013**, *56*, 6495.
22. Sharma, M.; Pandey, S.; Chauhan, K.; Sharma, D.; Kumar, B.; Chauhan, P. M. S. *J. Org. Chem.* **2012**, *77*, 929.
23. Desroses, M.; Scobie, M.; Helleday, A. *New J. Chem.* **2013**, *37*, 3595.
24. Shaabani, A.; Maleki, A.; Mofakham, H. *Synth. Commun.* **2008**, *38*, 3751.
25. Yang, L.; Shi, D.; Chen, S.; Chai, H.; Huang, D.; Zhang, Q.; Li, J. *Green Chem.* **2012**, *14*, 945.
26. Parish, H. A.; Gilliom, R. D.; Purcell, W. P.; Browne, R. K.; Spirk, R. F.; White, H. D. *J. Med. Chem.* **1982**, *25*, 98.
27. Haikarainen, T.; Venkannagari, H.; Narwal, M.; Obaji, E.; Lee, H.-W.; Nkizinkiko, Y.; Lehtiö, L. *PLoS One* **2013**, *8*, e65404.
28. Narwal, M.; Fallarero, A.; Vuorela, P.; Lehtiö, L. *J. Biomol. Screen.* **2012**, *17*, 593.
29. Venkannagari, H.; Fallarero, A.; Feijs, K. L. H.; Lüscher, B.; Lehtiö, L. *Eur. J. Pharm. Sci.* **2013**, *49*, 148.
30. Narwal, M.; Haikarainen, T.; Fallarero, A.; Vuorela, P. M.; Lehtiö, L. *J. Med. Chem.* **2013**, *56*, 3507.
31. Kabsch, W. *Acta Crystallogr. D Biol. Crystallogr.* **2010**, *66*, 125.
32. Vagin, A.; Teplyakov, A. *Acta Crystallogr. D Biol. Crystallogr.* **2010**, *66*, 22.
33. Dodson, E. J.; Winn, M.; Ralph, A. *Meth. Enzymol.* **1997**, *277*, 620.
34. Murshudov, G. N.; Skubák, P.; Lebedev, A. A.; Pannu, N. S.; Steiner, R. A.; Nicholls, R. A.; Winn, M. D.; Long, F.; Vagin, A. A. *Acta Crystallogr. D Biol. Crystallogr.* **2011**, *67*, 355.
35. Emsley, P.; Cowtan, K. *Acta Crystallogr. D Biol. Crystallogr.* **2004**, *60*, 2126.
36. Willert, K.; Brown, J. D.; Danenberg, E.; Duncan, A. W.; Weissman, I. L.; Reya, T.; Yates, J. R.; Nusse, R. *Nature* **2003**, *423*, 448.
37. Veeman, M. T.; Slusarski, D. C.; Kaykas, A.; Louie, S. H.; Moon, R. T. *Curr. Biol.* **2003**, *13*, 680.
38. Lau, T.; Chan, E.; Callow, M.; Waaler, J.; Boggs, J.; Blake, R. A.; Magnuson, S.; Sambrone, A.; Schutten, M.; Firestein, R.; Machon, O.; Korinek, V.; Choo, E.; Diaz, D.; Merchant, M.; Polakis, P.; Holsworth, D. D.; Krauss, S.; Costa, M. *Cancer Res.* **2013**, *73*, 3132.
39. Nathubhai, A.; Wood, P. J.; Lloyd, M. D.; Thompson, A. S.; Threadgill, M. D. *ACS Med. Chem. Lett.* **2013**, *4*, 1173.
40. Kumpan, K.; Nathubhai, A.; Zhang, C.; Wood, P. J.; Lloyd, M. D.; Thompson, A. S.; Haikarainen, T.; Lehtiö, L.; Threadgill, M. D. *Bioorg. Med. Chem.* **2015**, *23*, 3013.
41. Shultz, M. D.; Kirby, C. A.; Stams, T.; Chin, D. N.; Blank, J.; Charlat, O.; Cheng, H.; Cheung, A.; Cong, F.; Feng, Y.; Fortin, P. D.; Hood, T.; Tyagi, V.; Xu, M.; Zhang, B.; Shao, W. *J. Med. Chem.* **2012**, *55*, 1127.
42. Larsson, E. A.; Jansson, A.; Ng, F. M.; Then, S. W.; Panicker, R.; Liu, B.; Sangthongpitag, K.; Pendharkar, V.; Tai, S. J.; Hill, J.; Dan, C.; Ho, S. Y.; Cheong, W. W.; Poulsen, A.; Blanchard, S.; Lin, G. R.; Alam, J.; Keller, T. H.; Nordlund, P. *J. Med. Chem.* **2013**, *56*, 4497.